ACS OMEGA

http://pubs.acs.org/journal/acsodf

Article

Evaluation of Hydrophilic and Hydrophobic Silica Particles on the Release Kinetics of Essential Oil Pickering Emulsions

Zhe Li,[†] Xiaoxia Jiang,[†] Hongning Liu, Ziheng Yao, Ao Liu, and Liangshan Ming*

Cite This: *ACS Omega* 2022, 7, 8651−8664

Read Online

ACCESS | Metrics & More | Article Recommendations | Supporting Information

ABSTRACT: Colloidal particle-stabilized emulsions have recently gained increasing interest as delivery systems for essential oils. Despite the use of silica particles in food and pharmaceutical applications, the formation and release of hydrophilic and hydrophobic silica particle-stabilized emulsions are still not well studied. Thus, in this study, the structures of hydrophilic (A200, A380, 244FP, and 3150) and hydrophobic (R202 and R106) silica were deeply characterized using the solid state, contact angle, and other properties that could affect the formation of emulsions. Following that, Mosla chinensis essential oil emulsions were stabilized with different types of silica, and their characteristics, particularly their release behavior, were studied. Fick's second law was used to investigate the mechanism of release. Additionally, six mathematical models were employed to assess the experimental data of release: zero-order, first-order, Higuchi, Hixson−Crowell, Peppas, and Page models. The release mechanism of essential oils demonstrated that diffusion was the dominant mechanism, and the fitting results for the release kinetics confirmed that the release profiles were governed by the Higuchi model. The contact angle and specific surface area were the key properties that affect the release of essential oils from emulsions. Hydrophilic A200 was found to be capable of delivering essential oils more efficiently, and silica particles could be extended to achieve the controlled release of bioactives. This study showed that understanding the impact of silica particles on the release behavior provided the basis for modulating and mapping material properties to optimize the performance of emulsion products.

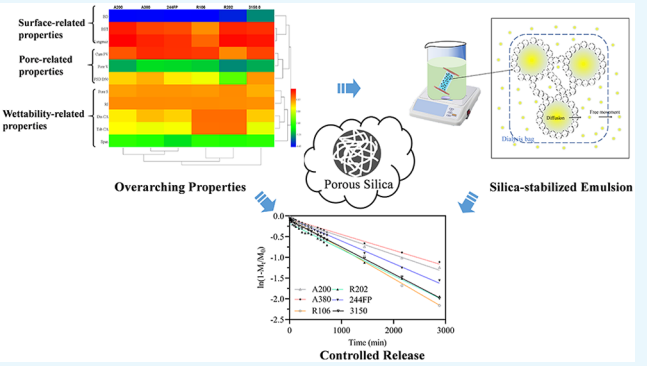

1. INTRODUCTION

Emulsions play an important role in overcoming the inherent problems of poorly water-soluble drugs or volatile bioactives and are extensively utilized in medicines[1] and functional foods.[2] Generally, large amounts of surfactants and other emulsifiers are added to the system to achieve the formation and stability of emulsions. However, excessive amounts of surfactants may have potential safety concerns for human health. Compared to the emulsions stabilized by conventional surfactants, emulsions stabilized by solid particles, often referred to as Pickering emulsions, have been widely used due to their unique emulsifying mechanism of a strong steric barrier at the interface, irreversible adsorption, and anchoring of solid particles.[3,4]

Pickering emulsions did not receive much attention at first due to the limited choice of solid particles. With the progress of science and technology, materials can be synthesized with adjustable properties and functions, thus allowing Pickering emulsions to be used widely in various fields. As an alternative to surfactants, solid silica particles have been proved to be an effective stabilizer in a variety of emulsion systems.[3,5] Many studies have been conducted on silica-stabilized emulsions, from the modification of the silica structure and function to the evaluation of emulsion stability. Silica particles were widely used in emulsions due to their surface chemistry, commercial availability, thermal stability, and low price.[6] Commercial silica particles, such as hydrophobic (e.g., Aerosil R805, Vacker H2000) and hydrophilic (e.g., Aerosil A300, Vacker N20) silica particles, have been used as potential stabilizers in the preparation of emulsions.[7,8] Also, the wettability of silica particles could be regulated by modification of functional groups. Alison et al. reported using chitosan to modify hydrophilic silica to improve its hydrophobic properties and promote its adsorption ability at the oil−water interface of emulsions.[9]

To date, many silica particles, both hydrophilic and hydrophobic, are available on the market. Some of the properties of these materials, such as wettability, porosity, surface area, density, and particle size, are key to drug delivery.[10] Despite the increasing applications in food and

Received: November 24, 2021
Accepted: February 18, 2022
Published: March 1, 2022

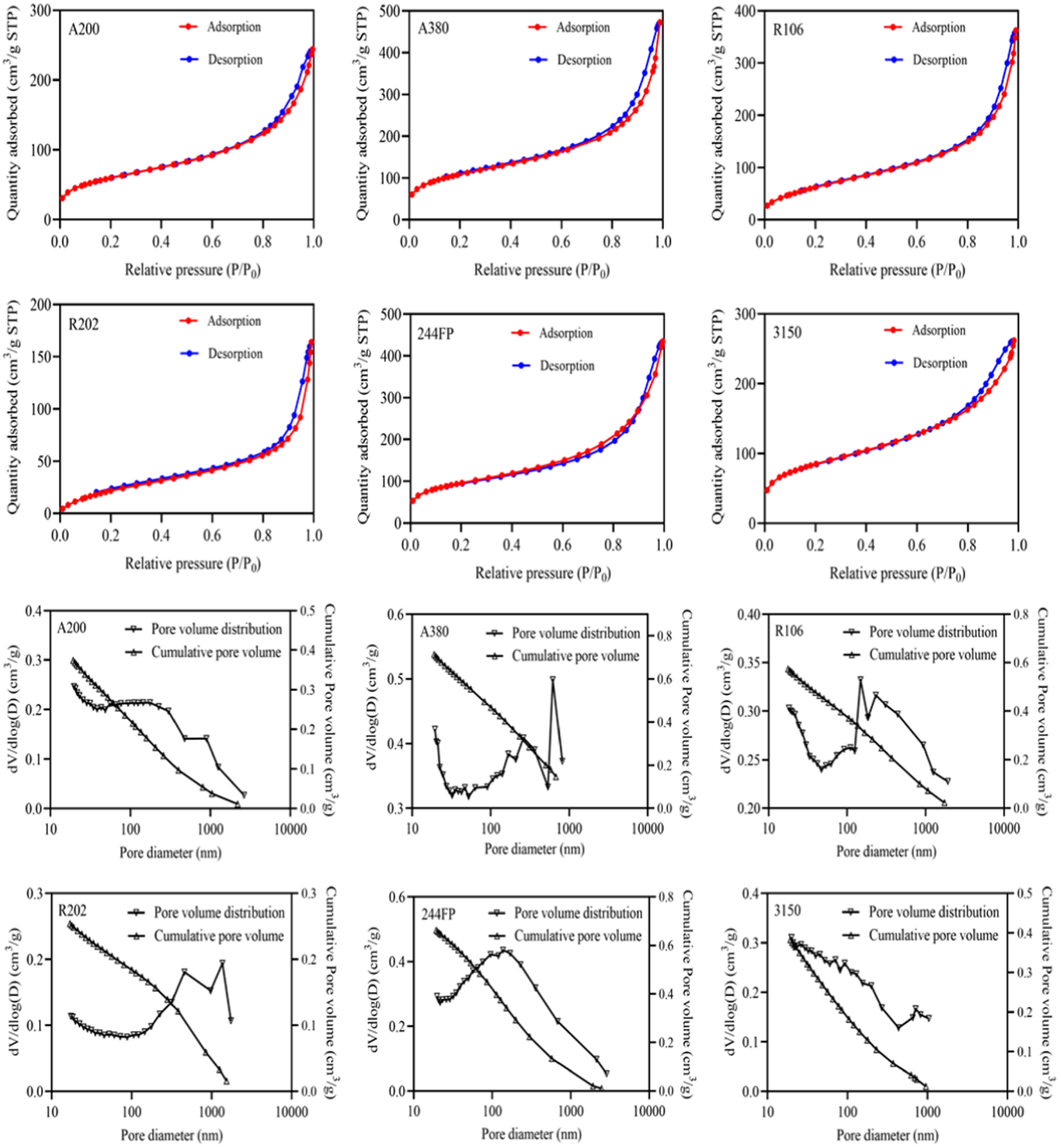

Figure 1. Nitrogen isothermal adsorption and pore size distribution curves of silica samples.

pharmaceutics, there is still only limited knowledge about the properties of silica in different specifications. Therefore, it is necessary to screen suitable silica to improve delivery efficiency. However, application of silica in pharmaceutical and food industries is still challenging because the related properties of silica obtained by different processes are unclear, and their subsequent application in pharmaceuticals and food is limited. The lack of related research on silica would lead to a deplorable ignorance of their potential values.

Essential oils have attracted great interest because of their excellent biological activities,[11] including antioxidant, anti-inflammatory, antibacterial,[12] and other health benefits.[13] Nevertheless, the application of direct incorporation of essential oils into products is still rare due to their poor physicochemical properties, such as hydrophobicity[14] and low solubility.[15] On the other hand, the sensitivity of essential oils to light, heat, and oxygen also limits their applications. Emulsions have been proven to be an effective strategy for enhancing the effective delivery of these substances while reducing the inherent issues.[16] A large number of essential oils such as oregano, cinnamon, basil, and thyme white have been

https://doi.org/10.1021/acsomega.1c06666
ACS Omega 2022, 7, 8651−8664

Table 1. Properties of Silica Samples

samples	BET specific surface area (m^2/g)	Langmuir specific surface area (m^2/g)	bulk density (g/cm^3)	$D[3.2]$ (μm)	span	dispersed contact angle (deg)	tablet contact angle (deg)	ratio of inner area (%)
A200	218.9911 ± 0.4460	305.4011 ± 6.5417	0.0473 ± 0.0001	9.704 ± 0.550	1.801 ± 0.231	29.6 ± 2.3	23.8 ± 1.1	99.26
A380	395.4748 ± 0.9762	534.6888 ± 10.1617	0.0489 ± 0.0001	19.371 ± 0.064	1.504 ± 0.044	54.2 ± 0.7	19.1 ± 2.0	99.19
R106	242.9380 ± 1.9994	354.9399 ± 11.5608	0.0499 ± 0.0001	25.169 ± 0.524	1.720 ± 0.017	144.1 ± 1.5	140.2 ± 1.1	99.91
R202	96.5682 ± 0.6862	156.4553 ± 5.3502	0.0476 ± 0.0003	18.303 ± 0.381	1.544 ± 0.098	143.9 ± 2.0	140.5 ± 1.8	98.18
244FP	345.5488 ± 1.2563	480.5328 ± 9.0660	0.0707 ± 0.0001	3.831 ± 0.257	0.747 ± 0.001	41.6 ± 1.7	22.0 ± 1.3	98.14
3150	305.5089 ± 1.2310	422.0394 ± 7.9852	0.2496 ± 0.0003	17.905 ± 0.847	1.760 ± 0.008	45.6 ± 3.6	17.6 ± 0.4	92.19

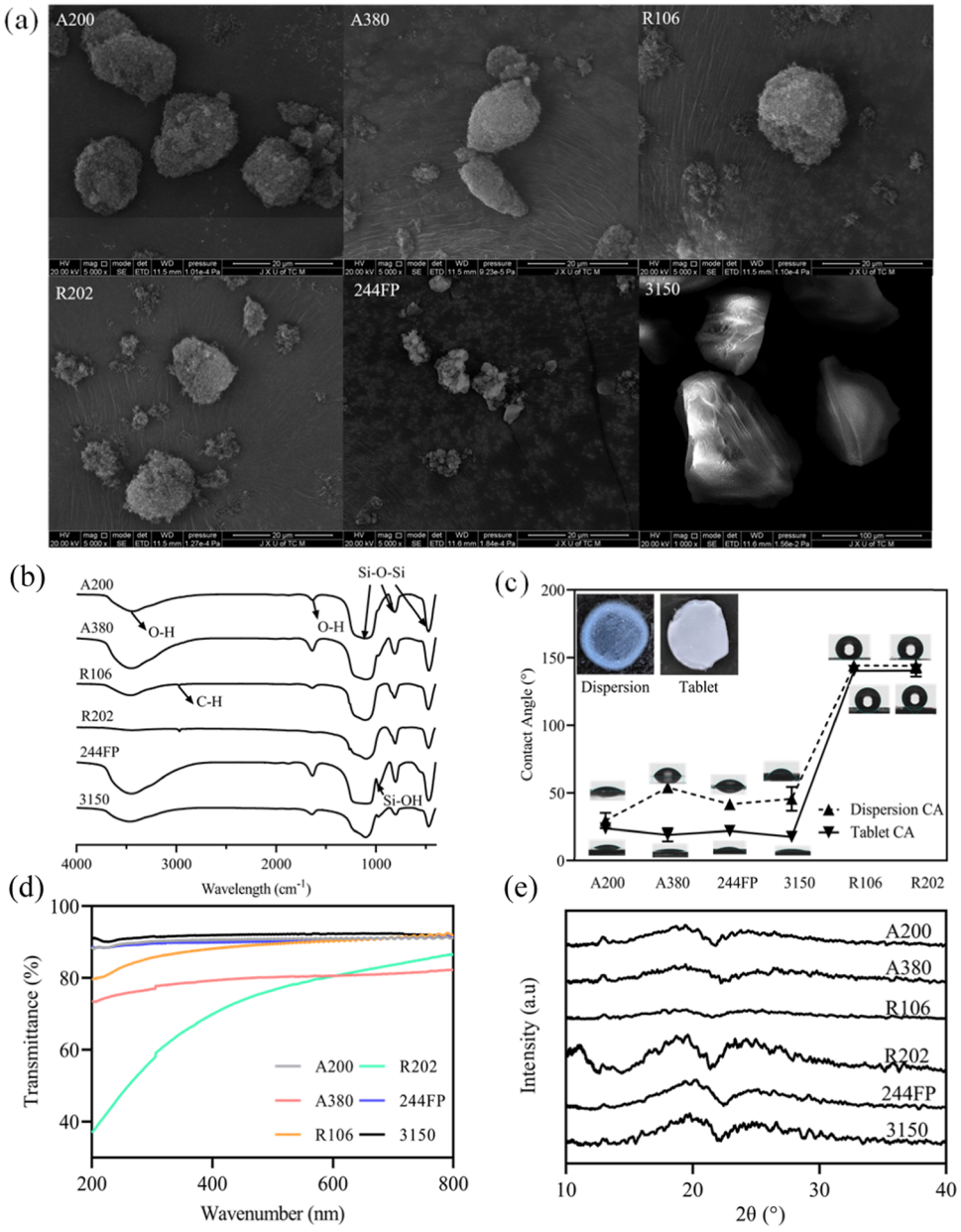

Figure 2. Properties characterization of different silica samples: (a) morphology and particle size distribution, (b) FT-IR, (c) contact angle with water, (d) transparency, and (e) XRD.

emulsified by particles of ZnO, nanocrystalline cellulose, etc., to enhance stability and biological activity.[17−19]

Based on all these considerations, this study aimed to evaluate the properties of commercially available silica samples and explore their potential as stabilizers for emulsions. To the best of our knowledge, no literature on the systematic study of different types of silica particles as emulsion stabilizers and for delivery of essential oils is available yet. Therefore, the specific research objectives of this study were to (a) identify overarching properties of six different types of silica samples, (b) examine the effect of different silica samples on the properties of emulsions and release profiles, and (c) investigate

https://doi.org/10.1021/acsomega.1c06666
ACS Omega 2022, 7, 8651−8664

the release mechanism of essential oils in silica-stabilized emulsions. For an enhanced understanding, the release kinetics of the essential oils from the fabricated emulsions was modeled. It is expected that the systematic study could clarify the suitability of different types of silica samples as potential carriers for emulsion systems, achieve the controllable release of essential oils, and finally expand the application of silica and essential oils in the fields of medicines and functional foods.

2. RESULTS AND DISCUSSION

2.1. Characterization of Silica Particles. The physicochemical properties of different samples were studied by various technologies to explore the differences in properties. Nitrogen isothermal adsorption is an effective strategy to characterize the specific surface area and pore size distribution of substances. From the isothermal adsorption/desorption curves (Figure 1), the trends of all kinds of silica curves were very similar, both of which had H3-type hysteresis loops and could be considered to belong to type II isotherm according to the IUPAC classification.[20] The occurrence of hysteresis loops was induced by multilayer adsorption and capillary coagulation of adsorption or desorption and was also caused by the presence of large pores.[21] The isothermal adsorption−desorption curves could be divided into three regions, namely, low pressure ($0 < P/P_0 \leq 0.2$) of the monolayer adsorption region, medium pressure ($0.2 < P/P_0 \leq 0.5$) of the multilayer adsorption region, and high pressure ($0.5 < P/P_0 \leq 1.0$) of the capillary condensation region. According to the specific surface area calculated from the adsorption curves based on the BET of multilayer adsorption and the Langmuir single-layer adsorption theories, the specific surface area values obtained by Langmuir were larger than that of BET, and these differences were caused by the different calculation principles. All of the silica samples exhibited large specific surface area values being 96 for R202 to 395 m^2/g for A380, which were calculated by the BET method (Table 1).

To obtain further insight information about the samples, their pore size characteristics, in terms of pore size distribution and cumulative pore volume, were characterized by the BJH model. It could be seen from Figure 1 that the pore diameter of all silica samples was mainly distributed in the range of 17−2000 nm, which indicated that the pore sizes of silica were mainly mesoporous (2−50 nm) and microporous (>50 nm), as recommended by the IUPAC standard.[22] From the curves, the pore size of silica samples was different. The average pore sizes of A200, A380, R106, R202, 244FP, and 3150 were 78.07, 88.58, 85.12, 99.30, 88.73, and 64.43 nm, respectively; and their corresponding pore volumes were 0.37, 0.71, 0.57, 0.25, 0.66, and 0.38 cm^3/g, respectively.

Moreover, 3150 exhibited the highest bulk density of 0.2496 g/mL, and A200 showed the lowest bulk density of 0.0473 g/cm^3 (Table 1). It had been confirmed that the bulk density of solid particles was also a key factor affecting the buoyancy and gravity of emulsions.[23] The smaller the density of the particles, the less the influence of gravity and the greater the influence of buoyancy, which contributed to the stability of the emulsion. Except for the 3105 sample, the density values of the other samples were less than 0.1 g/cm^3, reflecting the porous characteristics of silica particles.

The SEM analysis of the series of silica exhibited porous nature and assembled into large aggregates (Figure 2a). A200, A380, R106, and R202 exhibited a similar morphology, with loose aggregates and cotton-like structures, but individual dispersing silica particles could also be seen. 244FP particles displayed an irregular with a polygonal shape. The 3150 particles showed a lamellar porous structure with larger aggregates. This result was consistent with previously reported results.[24]

FT-IR data showed the characteristic groups of the silica powders (Figure 2b). The bands at ∼470, 800, and 1100 cm^{-1} observed for all of the samples were attributed to bending, rocking, and antisymmetric stretching vibrations of Si−O−Si.[25] Besides that, bands of the O−H group at ∼3400 and ∼1640 cm^{-1} were observed for the deformation vibrations of the adsorbed water molecules.[26] The bonds at ∼960 and 1940 cm^{-1} showed the presence of Si−OH and C−H groups, respectively. Because of the hydrophilic nature, samples A200, A380, 244FP, and 3150 had a strong and wide absorption peak at 3400 cm^{-1}, which was due to the absorption of water from the atmosphere. In contrast, hydrophobic samples R106 and R202 had weak absorption at 3400 cm^{-1}.

Wetting, an important parameter for emulsion preparation, was characterized by the contact angle (Figure 2c). Both dispersion and tableting methods were used to characterize the contact angle between silica and water. The contact angles of samples measured by the dispersion method were larger than those by tableting. The tableting method was commonly used because it could form a smooth surface and facilitate the measurement of contact angle. Our previous study had shown that when the contact angle was determined by the tableting method, the contact angle could be maintained only after a certain high pressure was reached (∼353 MPa).[27] At low tableting pressure, the capillary in the tablet would be attractive for probing liquid, thus underestimating the measurement of the contact angle. The contact angles of A200, R202, and R106 showed no difference between the two methods, but the contact angles of A380, 244FP, and 3150 samples were significantly higher by the dispersion than by the tableting method. Considering that the contact angle might be reduced due to the capillary action by the tableting method, the dispersion method could be used as a supplement to the contact angle measurement. It was thought that the dispersion method could better maintain the microstructure of the silica samples. As expected, the two hydrophobic silica samples, R106 and R202, had the maximum contact angles of 144.1 and 143.9°, respectively, indicating strong hydrophobic nature. Compared with the other four kinds of silica, R106 and R202 had poor wettability and strong hydrophobic sites, penetrating the oil phase more easily.[28] In contrast, the contact angles of other silica samples ranged from 29.6 to 54.2°, showing that materials were hydrophilic as well as partially hydrophobic.

Transparency was an important physical parameter that could be used to analyze the optical properties of silica samples, as shown in Figure 2d. Samples 3150, 244FP, and A200 expressed the highest transmittance in the range from 200 to 800 nm, and transmittance was over 90%. As for R106, the transmittance was over 90% between 400 and 800 nm and decreased to 80% in 400−200 nm. A similar trend occurred with sample A380. However, the signal of R202 showed an upward trend with the increase of wavelength, and the transmission gradually increased from 37 to 88% in a wavelength range from 200 to 800 nm.

The solid state of silica samples was characterized using X-ray diffraction, as shown in (Figure 2e). The structures of all the silica samples were still amorphous with broad bands; no crystal structure appeared in these samples. Previous studies

https://doi.org/10.1021/acsomega.1c06666
ACS Omega 2022, 7, 8651−8664

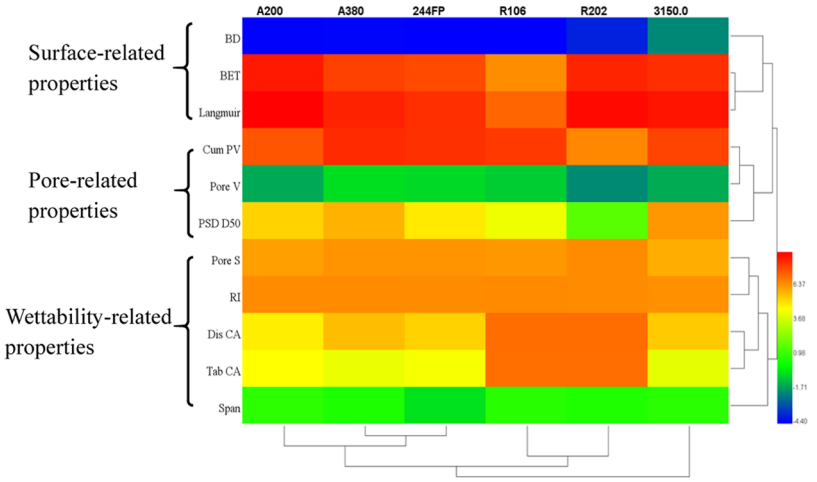

Figure 3. Hierarchical clustering heatmap analysis of the silica samples related to different properties. The dendrograms are based on the Euclidean linkage algorithm. BD: bulk density; BET: BET specific surface area; Langmuir: Langmuir specific surface area; Cum PV: cumulative pore volume; PSD D50: medium value of particle size distribution; Pore S: pore size; RI: ratio of the inner area; Dis CA: dispersed contact angle; Tab CA: tablet contact angle; and Span: (D90-D10)/D50.

showed that fumed silica particles exhibited a typical amorphous shape in the XRD.[29]

Primary hydrophilic silica particles with primary sizes between 5 and 30 nm were provided by the manufacturer.[30] After that, the powders aggregated into larger units about submicron and several microns (Table 1). The difference between the measured particle and that of primary size could be ascribed to the aggregation of the particles inherently taking place in dry nanopowders.[31] However, in the preparation process of emulsions, the aggregated silica particles could be dispersed into the nanoscale, and the particle size of dispersion in aqueous solutions was about 150 nm, as described in the literature.[32] The $D[3.2]$ of the series silica was generally less than 30 μm, varying from a minimum of 3.8 μm for 244FP up to a maximum of 25.2 μm for R106. The span reflected the degree of particle size uniformity. 244FP had the most concentrated particle size distribution with a span of 0.74, while the span of the other silica was between 1.5 and 1.8. Besides, the ratio of the inner area was calculated based on the specific surface areas and median particle sizes of the samples. As expected, all samples had very high inner surfaces (>92%), indicating that the samples had a lot of porosity inside, which was consistent with the results of pore size distribution.

Ultimately, a heatmap was constructed for data mining to illustrate the difference among the samples intuitively.[33] The heatmap, an effective practical tool for processing complex data, was used to make the data understandable and actionable and to explore the mechanisms behind the data.[34] The heatmap hierarchical clustering of physicochemical properties was analyzed based on similarities and differences, including bulk density, specific surface area, pore volume, pore size, particle size distribution, and contact angle (Figure 3). As a data visualization tool, in this study, red represented higher values in the heatmap, whereas blue represented lower values, which provided a more visual data trend. Consistent with previous studies, silica samples from different manufacturers and brands displayed different properties.[35] For different kinds of silica samples, it was clear that the original 11 variables could be condensed and reduced into three overarching properties, which were classified according to Pearson distance similarity. The first cluster was identified as surface-related properties, whereas the second and third could be attributed to pore-related properties and wettability-related properties. Similarly, different types of silica could also be divided into three categories based on the differences and similarities in properties. Hydrophilic A200, A380, and 244FP samples could be combined into one category, hydrophobic R106 and R202 were divided into one category, and finally, hydrophilic 3150 was one category. The first two categories were well understood because of the hydrophilic and hydrophobic nature of samples. The reason why sample 3150 was in a separate category was that it had the largest bulk density and particle size values, which were far greater than those of other samples. It was speculated that the difference in the properties of silica samples would affect the properties of silica-stabilized emulsions.

2.2. Essential Oil Isolation and Analysis. In this section, the chemical compositions of the essential oil of dried *Mosla chinensis* herbal were determined. *Mosla chinensis* 'Jiangxiangru' was widely used in food supplements and folk medicine for its antibacterial, anti-inflammatory, antiviral, and antioxidant properties. In traditional medicine, this herb has been used for diaphoresis and influenza. This plant is widely grown in the southern provinces of China, Vietnam, India, and Japan.[36] Jiangxi province in China is its main producing area. As a potential functional food with medicinal value, its leaves are widely considered as a wild vegetable to be eaten or a food supplement to give aroma and flavor.[37] The chemical composition of the essential oil was isolated by water hydrodistillation and analyzed by GC-MS, and the results are shown in Table 2 and Figure 4. A total of 11 compounds were identified in the essential oil. The predominant compounds were carvacrol (75.40 ± 0.06%), thymol (11.04 ± 0.04%), and cymene (5.14 ± 0.02%). A similar result was presented in the research of Cao et al., and the main compounds in their study identified were carvacrol (57.08%), thymol (6.67%), and cymene (13.61%).[37] The essential oil reported in this paper had a higher carvacrol content, and this discrepancy was attributed to the climatic conditions, growth location, the extraction method of essential oil, etc.[38]

2.3. Characterization of Emulsions. Camellia oil was chosen as the oil phase for this study since it is edible[39] and

https://doi.org/10.1021/acsomega.1c06666
ACS Omega 2022, 7, 8651−8664

Table 2. Chemical Composition of Essential Oils

no.	compounds	relative peak area (%)
1	β-myrcene	0.38 ± 0.01
2	α-terpinene	0.51 ± 0.01
3	cymene	5.14 ± 0.02
4	eucalyptol	0.19 ± 0.01
5	γ-terpinene	1.31 ± 0.01
6	terpinen-4-ol	0.71 ± 0.01
7	carvacrol	75.40 ± 0.06
8	thymol	11.04 ± 0.04
9	bergamotene	0.11 ± 0.01
10	α-humulene	0.92 ± 0.01
11	caryophyllene oxide	0.41 ± 0.01

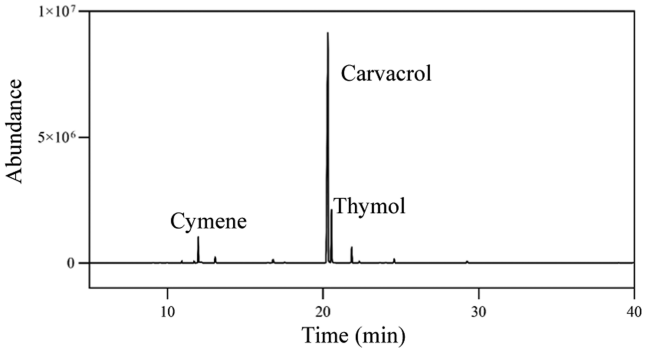

Figure 4. Total ion chromatograph for GC-MS detection of essential oils.

most commonly available in foods and drugs.[40] At the same time, camellia oil was also an oil solvent for injection and had good safety.[41] Therefore, it could be used as the oil phase of emulsions to deliver poorly soluble and unstable bioactives. The properties of emulsion systems stabilized by several kinds of silica were compared.

The change in Pickering emulsion rheology based on different kinds of silica was evaluated (Figure 5). The viscosity

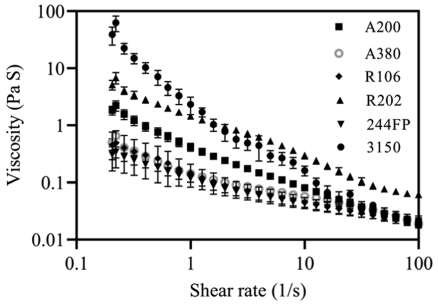

Figure 5. Viscosity as a function of shear rate for the silica-stabilized Pickering emulsions.

decreased as the shear rate increased, indicating that the emulsion exhibited shear thinning behavior, similar to most reported emulsions.[42] Encapsulation efficiency values for emulsions ranged between 20.97 and 58.70%, evidencing statistical significances (Table 3). The lowest encapsulation efficiency was obtained for the R202-stabilized emulsion (20.97%), and the highest percentage of entrapment efficiency was obtained for the A200-stabilized emulsion (58.7%). It was speculated that the structure and physical properties of silica samples as well as their preparation conditions affected the ability of an emulsion to encapsulate and retain essential oils. Emulsions were formed via hydrogen bonding, van der Waals forces, electrostatic forces, and mechanical barriers.[43] The properties of silica, such as particle size, porosity, density, and wettability, would alter the forces mentioned above and thus affect the emulsions for the encapsulation of essential oils.

The typical microscopic images of the droplets of silica-stabilized emulsions were observed. Figure 6 shows the optical microscopy of typical emulsions. A spherical dispersed droplet structure could be observed for all emulsions. The immiscibility behavior of the oil layer and the water layer could be easily distinguished (Figure S1). Average droplet size values were 20.3, 26.5, 35.3, 33.9, 32.4, and 24.2 μm for A200, A380, R106, R202, 244FP, and 3150, respectively (Table 3). The droplet size was related to the inherent properties of the oil phase, such as the chemical structure and physical and chemical properties, and was also associated with the stability of emulsions.[44]

2.4. Release Profile and Effective Diffusivity Analysis.

Essential oils have recently been extensively studied as additives of antioxidants, antimicrobials, antidiabetic, and anti-inflammatory activates in the pharmaceutical, food, and cosmetics industries.[45] However, the strong hydrophobicity and volatile defects of essential oils have become major obstacles in their applications. Therefore, increasing the stability and availability of essential oils and realizing effective delivery were the prerequisites for food and pharmaceutical applications. Emulsion-based delivery systems are considered an effective strategy to increase the dispersion, stability, and bioavailability of therapeutic substances.

It had been demonstrated that in Pickering emulsions, large interfacial gaps between particles enable the encapsulation material to diffuse from the inner phase.[46] The release profiles obtained from the emulsions with different silica stabilizers are shown in Figure 7a. It could be seen that the release of essential oil in the emulsion increased with the increase of time. Release curves showed that the release of essential oil was faster from hydrophobic silica samples such as R202- and R106-stabilized emulsions than from other hydrophilic emulsions. After 24 h, all emulsions released nearly 50% of the essential oil (Table 3). At 24 h, the highest release of essential oil was 67.58% for the emulsion with the R202

Table 3. Properties of Emulsions Using Different Silica Samples as Stabilizers

	$D[3.2]$ (μm)	viscosity (mPa S)	encapsulation efficiency (%)	release in 24 h (%)	D_{eff} (μm^2/min)
A200	20.379 ± 1.356	0.0192 ± 0.0011	58.70 ± 3.69	52.30 ± 1.50	0.004513
A380	26.474 ± 0.947	0.0189 ± 0.0011	56.03 ± 1.58	48.33 ± 2.87	0.006753
R106	35.298 ± 1.525	0.0186 ± 0.0025	52.51 ± 6.32	62.07 ± 0.48	0.023009
R202	33.946 ± 3.080	0.0615 ± 0.0061	20.97 ± 1.02	67.58 ± 4.28	0.018358
244FP	32.397 ± 0.607	0.0199 ± 0.0039	48.78 ± 7.08	59.32 ± 1.59	0.014419
3150	24.248 ± 0.126	0.0216 ± 0.0042	51.35 ± 7.35	63.94 ± 1.93	0.005277

https://doi.org/10.1021/acsomega.1c06666
ACS Omega 2022, 7, 8651−8664

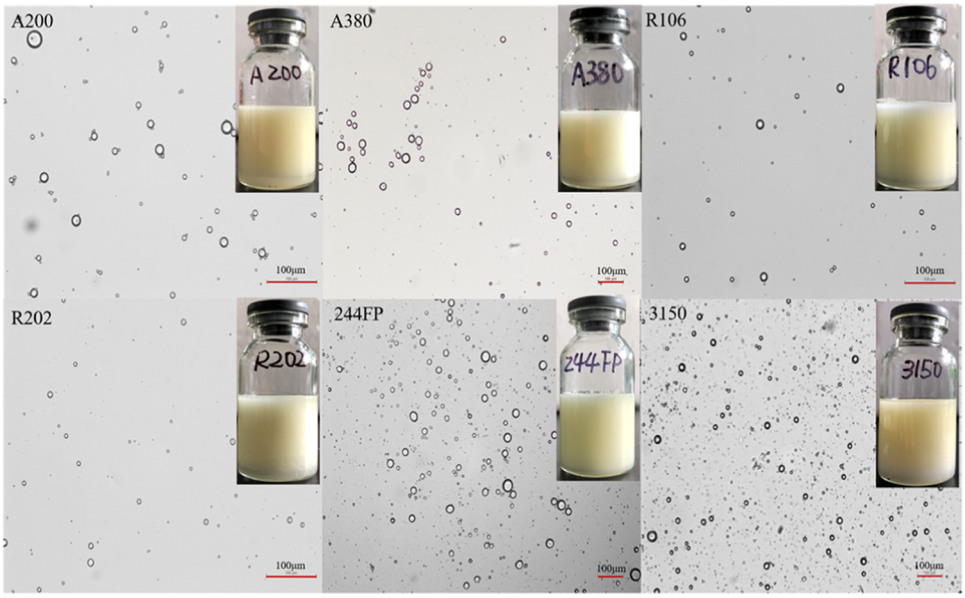

Figure 6. Visual appearance and microscopic images of silica-stabilized Pickering emulsions.

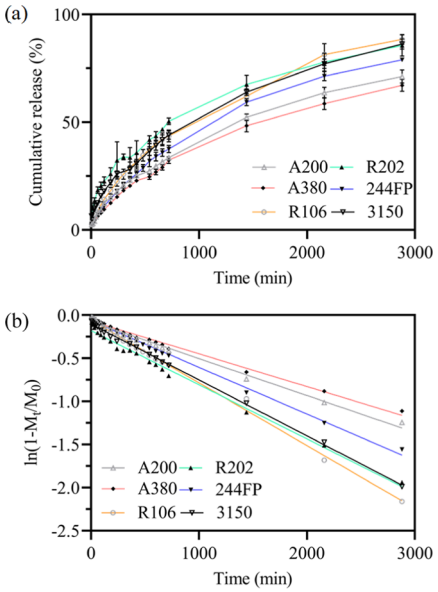

Figure 7. In vitro release profile of essential oil from silica-stabilized Pickering emulsions: (a) cumulative percentage of essential oil release and (b) diffusion coefficient fitting.

stabilizer, while the lowest release was observed at 48.33% for the A380-stabilized emulsion. It was suggested that the type of silica samples played a significant role in the rate of bioactive release from emulsions, and the controlled release could be achieved by only altering the type of silica.

In an attempt to further explore the difference in essential oil release from emulsions that were stabilized by different kinds of silica, Fick's diffusion law was applied to calculate the diffusion coefficients. This approach has been used in previous studies to investigate the mechanism of bioactive release from emulsions.[47] It was assumed that the small molecule entities could pass the dialysis membrane freely and that the diffusion from the emulsion was the rate-limiting step.

Therefore, the mathematical model based on Fick's diffusion could be fitted and further used to calculate the effective diffusion coefficient. Figure 7b shows that the linear fitting results of all release curves were satisfactory. The gradient of the resulting linear fit could be used to calculate the diffusion coefficient, as shown in Table 3. Diffusion coefficients reflected the release rate of essential oil from the emulsions. The effective diffusivity values were found to vary in the range of 0.0045−0.0230 μm^2/min. The calculated diffusivities were 0.004513, 0.006753, 0.023009, 0.018358, 0.014419, and 0.005277 μm^2/min for A200-, A380-, R106-, R202-, 244FP-, and 3150-based emulsions, respectively. The essential oil was released from emulsions in a controlled manner, with the release rate increased in an order of A200 < 3150 < A380 < 244FP < R202 < R106. The greater release effect of R106 could be reasonably attributed to its hydrophobic properties and relatively small specific surface area with respect to the other hydrophilic character of silica samples. It has been recently described by other authors that the physicochemical properties and surface area of the oil−water interface layer had a major influence on the rate and extent of the release of active ingredients.[48]

On the premise of elucidating the related mechanism, silica-stabilized emulsions with different properties could be fabricated to realize the controlled release of bioactives. The above comprehensive results also showed that the properties of silica could affect the structure of emulsions and the release of bioactives in emulsions. Therefore, exploring the internal relationship between the structure/physicochemical properties of silica samples and the properties of emulsions would be an important basis for regulating the function of silica-stabilized emulsions.

2.5. Effect of Key Properties of Silica Particles on Effective Diffusivity. Model fitting was performed using stepwise regression involving six factors (BET specific surface area, bulk density, particle size $D[3.2]$, span, dispersed contact angle, and ratio of inner area) as independent variables. The results of the statistical analysis using SAS-JMP in leverage plots and the summary of fit are shown in Figure 8 and Table 4, respectively. The leverage plots for the linear effect were a simple regression and a point farther from the center of the plot in the horizontal direction contributed a greater influence

https://doi.org/10.1021/acsomega.1c06666
ACS Omega 2022, 7, 8651−8664

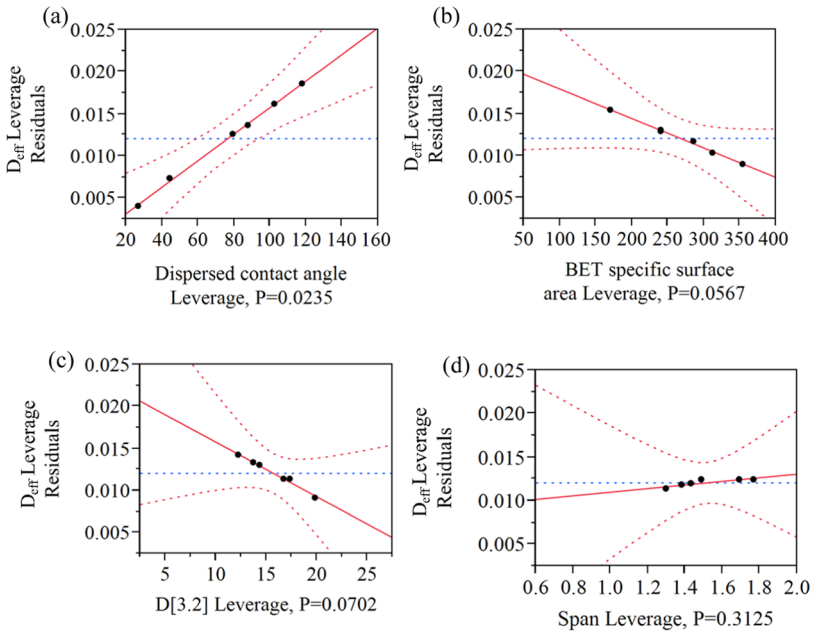

Figure 8. Effects of the main physical properties on effective diffusivity: (a) leverage plot of the contact angle, (b) leverage plot of the specific surface area, (c) leverage plot of $D[3.2]$, and (d) leverage plot of span.

Table 4. Statistical Summary of the Fit of Effective Diffusivity[a]

summary of fit		parameter estimates		
		term	estimate	prob > |t|
R^2	0.9993	intercept	0.00164	0.0359**
adjusted R^2	0.9965	SSA	−0.00004	0.0567*
RMSE	0.0005	$D[3.2]$	−0.00065	0.0702*
		span	0.00021	0.3125
		contact angle	0.00016	0.0235**

[a]*P < 0.10; **P < 0.05; and SSA, BET specific surface area.

on the fitting.[49] Additionally, statistical parameters such as the square of the correlation coefficient (R^2), root mean square error (RMSE), parameter estimates, and their significance (P-values) were used to test the fitting accuracy.[50]

From the leverage plots in Figure 8 and the summary of statistical analysis in Table 4, the R^2 (0.9993) and adjusted R^2 (0.9965) values were reasonably high and RMSE (0.0005) was low, indicating that the model had good accuracy. The effect of the specific surface area, span, contact angle, and $D[3.2]$ on the effective diffusivity of emulsion release was evaluated by the effect leverage plots, which depicted how the above independent variables affected the effective diffusivity and gave insights into the multicollinearity of the statistical model.[51] In the effect leverage plots, the small P-values combined with the results that 95% confidence curves (red dotted lines in the figure) crossed the hypothetical horizontal line (blue dotted line in the middle of the figure) showed that both the specific surface area and contact angle were significant (Figure 8a,b), while the large P-values for span (0.3125) had nearly no effect on the effective diffusivity (Figure 8d), which supported the results of statistical analysis (Table 4).

The stepwise regression model revealed that both the specific surface area and contact angle had significantly contributed to the effective diffusivity. Interestingly, the effective diffusivity was positively correlated to the contact angle and negatively correlated to the specific surface area. Parameter estimates showed that the contact angle had a more significant influence (0.00016) than the specific surface area (−0.00004) (Table 4).

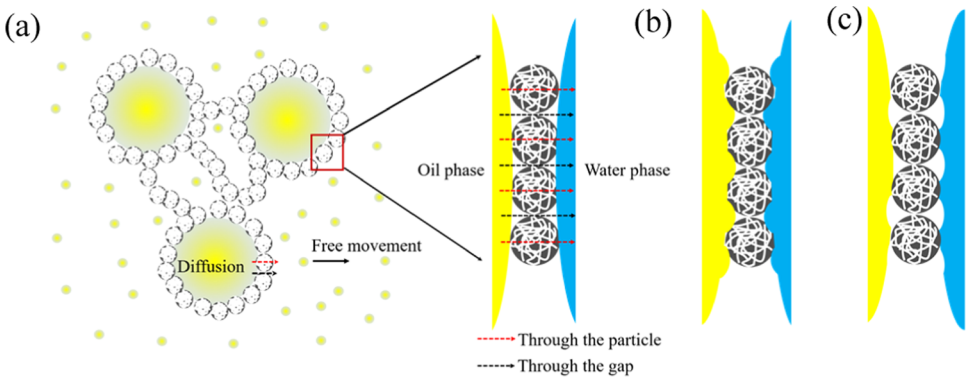

Figure 9. Schematic diagram for release mechanism of essential oil in Pickering emulsions: (a) bioactive release mechanism from the droplet, (b) oil−water interface at a low contact angle, and (c) oil−water interface at a high contact angle.

https://doi.org/10.1021/acsomega.1c06666
ACS Omega 2022, 7, 8651−8664

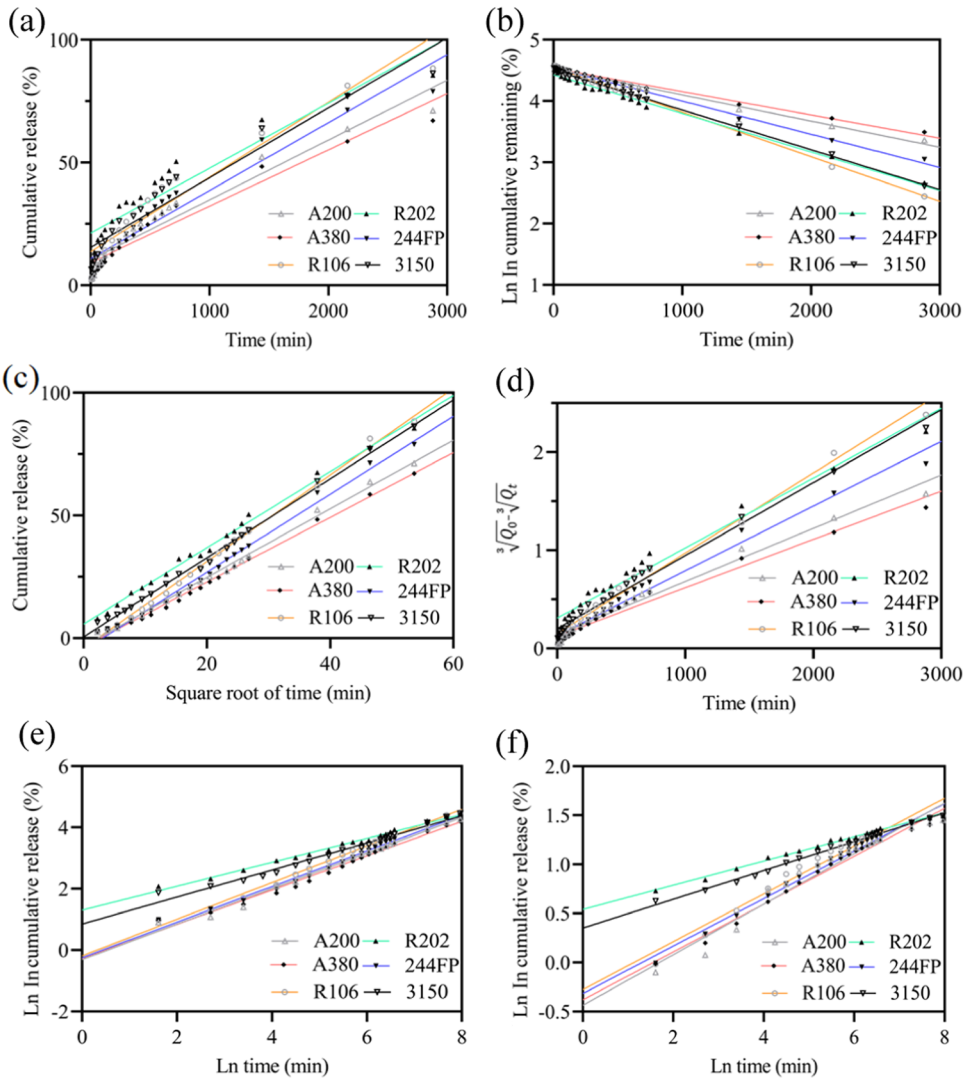

Figure 10. Fitting the release profiles with different models: (a) zero order, (b) first order, (c) Higuchi, (d) Hixson−Crowell, (e) Peppas, and (f) Page.

It should be noted that the release of bioactives from the emulsions was mainly the migration of bioactives from the oil phase through the particles bridging to the water phase, which was closely related to the densely distributed particles bridging at the oil−water interface. Therefore, a representative diagram could be used to depict the possible emulsion formation pathway and release process (Figure 9a). The contact angle was the most important factor for effective diffusivity as shown by a higher parameter estimate. Increasing contact increased the effective diffusivity of emulsions. For the stability of the emulsion, the interfacial attachment energy of particles to the two-phase interface was the key parameter.[52] The higher the attachment energy, the better the stability of the emulsion. Lower interfacial tension, moderate contact angle, particle content, etc., were beneficial to the preparation of emulsions. But in practice, higher attachment energy might also lead to the instability of the emulsion because there were other factors such as surface charge and morphology of particles that could affect the stability.[53]

$$E = \pi\left(\frac{d}{2}\right)^2 \gamma(1 + \cos\theta)^2$$

where E is the attachment energy, d is the diameter of the particle, γ is the interfacial tension between the oil and water phases, and θ is the contact angle at the oil−water interface.

Increasing the contact angle promoted the release of bioactives. The possible reason could be attributed to the reduction of the contact surface between particles and the oil−water interface and the gap widened as the contact angle increased, making the bioactives more easily penetrate the oil−water interface through the gap (Figure 9b,c). In contrast to the contact angle, the specific surface area had an adverse effect on bioactive release. As the internal porosity of silica was as high as over 92%, the high specific surface area was mainly due to the abundance of internal voids of silica particles. In the case of equivalent particle size, the larger specific surface area of silica involved more voids and more complex internal channels, which needed to pass through the sinuous pathway before bioactives could be released. At the same time, studies have confirmed that hollow particles with a high specific surface area had strong attachment energy and made the emulsion more stable.[23]

2.6. Mathematical Modeling of Release Curves. The dissolution kinetics was assessed by fitting the experimental data to the models. In this study, six commonly used release

https://doi.org/10.1021/acsomega.1c06666
ACS Omega 2022, 7, 8651−8664

Table 5. Fitting Parameters of the Curves for the Different Models

	zero-order		first-order		Higuchi		
	k	R^2	k ($\times 10^{-4}$)	R^2	k	n	R^2
A200	0.02440	0.9295	4.269	0.9897	1.400	−3.258	0.9962
A380	0.02296	0.9318	3.794	0.9874	1.321	−3.599	0.9949
R106	0.03048	0.9135	7.283	0.9952	1.765	−4.101	0.9968
R202	0.02651	0.8886	6.283	0.9912	1.554	5.743	0.9941
244FP	0.02772	0.9264	5.418	0.9953	1.590	−4.964	0.9922
3150	0.02847	0.9298	6.492	0.9982	1.611	0.490	0.9963
	Hixson−Crowell		Peppas			Page	
	k ($\times 10^{-4}$)	R^2	k	n	R^2	k	n	R^2
A200	5.425	0.9756	0.7318	0.5798	0.9880	−0.6464	0.2576	0.9527
A380	4.924	0.9736	0.7556	0.5597	0.9825	−0.6838	0.2438	0.9823
R106	8.168	0.9862	0.8279	0.5976	0.9932	−0.7592	0.2436	0.9627
R202	7.127	0.9699	3.6877	0.3896	0.9918	−1.7188	0.1231	0.9939
244FP	6.596	0.9810	0.7780	0.5810	0.9874	−0.7286	0.2419	0.9821
3150	7.441	0.9892	2.3392	0.4406	0.9803	−1.4205	0.1467	0.9938

models for fitting procedures for the release profiles are shown in Figure 10, and their correlation parameters are shown in Table 5. The best-fitting models were Higuchi > first order > Peppas > Page > Hixson−Crowell > zero order. The regression values of R^2 for the Higuchi release model were between 0.9922 and 0.9968, confirming that the release of essential oil from emulsions could be attributed to diffusion throughout the matrix and followed Fick's second law. Fick's diffusion always occurred in the case of porous matrix[54] and microemulsion systems.[55] In our previous work, the Page model was more suitable to fit the release kinetics of the cyclodextrin inclusion complex, while in this study, Higuchi had a higher model accuracy, indicating that the existing form of bioactives could affect the release. In the inclusion complex, bioactives were encapsulated in supramolecular structures, and in emulsions, bioactives were highly dispersed into droplets.[56] Differences in these structures resulted in different release mechanisms.

3. CONCLUSIONS

To date, many kinds of silica particles have been used to fabricate Pickering emulsions. However, the properties of different kinds of silica have not been studied systematically, and the effect of these properties on the emulsions was still unknown. Therefore, our aim was to study how the type of the silica samples modulate the formation and release of emulsions. Preliminary in-depth characterization of the properties of silica was carried out by various technologies. After that, the suitability of different kinds of silica samples as potential emulsion carriers for the delivery of essential oils was evaluated. The release mechanism of essential oils from silica-stabilized emulsions was suggested to be Fickian, depending on the molecular diffusion. The release profiles were fitted by six different models, and the release kinetics showed that the release of essential oils from silica-stabilized emulsions was followed the Higuchi model, based on statistical analysis. Based on the results of the performance of the emulsions and the release kinetics, A200 silica particles were the most effective carriers to achieve the enhanced performance of essential oils in the emulsion. In summary, efficient encapsulation and controlled release of essential oils could be achieved by selecting suitable silica particles.

4. METHODS

4.1. Materials. Hydrophilic Aerosil 200 (A200) and Aerosil 380 (A380) and hydrophobic Aerosil R202 (R202) and Aerosil R106 (R106) silica samples were manufactured by Evonik Degussa, provided by Kingchemical (China). Hydrophilic Syloid 244FP (244FP) and Syloid XDP 3150 (3150) were kindly supplied by Grace GmbH (Germany). All silica samples were supplied in the solid powder form. Deionized water was prepared by a Milli-Q water system. Mosla chinensis 'Jiangxiangru' was provided by Jiangzhong TCM Pieces (China), and its essential oil was obtained by hydrodistillation. Camellia oil as the oil phase was purchased from Jiangzhong Food Therapy (China), and its fatty acid composition was 11% saturated fatty acid, 79.5% monounsaturated fatty acid, and 9.5% polyunsaturated fatty acid. All other reagents were of analytical grade. Dialysis cassettes (molecular weight cutoff of 2 kDa) were purchased from Solarbio (China). All reagents were used without further purification.

4.2. Characterization of Silica Samples. The isothermal nitrogen adsorption/desorption curves were measured on a TriStar 3000 surface area analyzer (Micromeritics) at 77K. The specific surface area was calculated by the Brunauer−Emmett−Teller (BET) and Langmuir models, and the pore volume and pore size distribution were obtained by the Barrett−Joyner−Halenda (BJH) model based on adsorption data. Prior to measurement, the samples were degassed at 80 °C for 5 h in a FlowPrep 060 Sample Degas System (Micromeritics).[57]

The morphology of silica samples was determined using a Quanta 250 scanning electron microscope (SEM). Before the measurement, each sample was sputter-coated with gold to increase electrical conductivity.[56]

Particle size distribution was determined using laser diffraction of a Mastersizer 2000 (Malvern, U.K.) with a Hydro 2000MU dispersion unit by dispersing the powder in water for hydrophilic samples or ethanol for hydrophobic samples.[57]

The bulk density (ρ) of the powder was measured by pouring the sample into a cylinder with a volume of 100 mL, scraping off the excess powder on the surface, weighing the mass, and calculating the bulk density as the ratio of mass occupied to the volume.[58]

https://doi.org/10.1021/acsomega.1c06666
ACS Omega 2022, 7, 8651−8664

When the particle was a sphere, the ratio of the inner area (RI) of the silica samples was calculated as the ratio between the specific surface area and the geometric area.[59]

$$RI = 100 \times \left(1 - \frac{S_{geo}}{S_{tol}}\right) = 100 \times \left(1 - \frac{6}{\rho S_{tol}}\right)$$

where d is the median particle size measured by laser diffraction, ρ is the bulk density, and S_{tol} is the total area calculated by the BET model.

Fourier transform infrared (FT-IR) spectra were collected in the range of 4000−400 cm^{-1} with a resolution of 4 cm^{-1} and 64 scans on a Spectrum Two Spectrophotometer (PerkinElmer, U.K.) using KBr pellet technology.[56]

Contact angle measurements were performed using an OCA20 contact angle analyzer (DataPhysics, Germany) and automatically calculated by a sessile drop method at room temperature. The sample was prepared either by compacting it into a tablet at 353 MPa[27] or dispersing it in *n*-hexane onto a glass slide at 10 mg/mL.[60] By powder particle compaction or evaporation of n-hexane, a relatively dense membrane of silica was preserved. For hydrophilic samples, 2 μL of deionized water was used as the detection liquid for the contact angle measurement, while for hydrophobic samples, 10 μL of deionized water was used.[61]

The transparency of silica samples was measured using a UV-2600 UV−vis spectrophotometer (Shimadzu, Japan) at a wavelength range from 200 to 800 nm.[62] Before measurement, the silica substrate was dispersed in n-hexane at a concentration of 10 mg/mL, and a silica membrane was formed and dispersed on the surface of a colorimetric dish when *n*-hexane was volatilized.

X-ray diffraction data were collected using an X-ray Oxford diffraction instrument XTaLAB Synergy-R diffractometer (Rigaku, Japan) equipped with a CCD detector, using Cu Kα radiation.[63]

4.3. Extraction and GC/MS Analysis of Essential Oil. *Mosla chinensi* essential oil (with low density < 1.0 g/mL) was extracted by water hydrodistillation using a Clevenger apparatus.[64] The dried herb was placed in distilled water (ratio w/v = 1/8) and extracted at 3 h. The chemical composition of essential oil was determined by gas chromatography and mass spectrometry (GC-MS, Agilent 5975). National Institute of Standards and Technology (NIST) v17 (Department of Commerce, Washington) as a standard library was utilized to analyze the ingredients of essential oil. The extracted oil was dissolved in HPLC grade methanol prior to the injection with a concentration of 10 μL/mL. In each analysis, about 1.0 μL of a diluted sample was injected into the GC/MS system equipped with a mass selective detector. The operating conditions were the following: a capillary column Agilent 123-1334 DB-624 (30 m × 320 μm × 1.8 μm); helium as a carrier gas: 1.0 mL/min; injector temperature: 250 °C; capillary column temperature programmed at 50 °C isothermals for 5 min, then increased to 80 °C at a rate of 1 °C/min and held isothermal for 2 min, increased to 150 °C at a rate of 5 °C/min isothermal for 2 min, and finally increased to 220 °C at a rate of 10 °C/min; split ratio: 1:50; ion source temperature: 230 °C; and mass scan range: 29−650 mass unit.

4.4. Emulsion Preparation and Characterization. Based on the results of preliminary experiments, the formulation of the emulsion was optimized. The emulsion comprised 50% oil phase and 50% aqueous phase. The oil phase was a solution of camellia oil and essential oil prepared in a volume ratio of 90:10. The mass fraction of silica added to the emulsion was fixed at 0.5% of the emulsion (m/v). The emulsion was emulsified using an FA 25 disperser (Fluko, Germany) operating at 13 000 rpm for 5 min in an ice bath.[65] The volume of the emulsions produced was 20 mL.

The Sauter surface-weighted mean diameter ($D[3,2]$) of droplets was determined by laser diffraction of a Mastersizer 2000 (Malvern, U.K.) with a Hydro 2000 MU dispersion unit.[66]

Rheological measurements of emulsions were performed with an MCR 101 Rheometer (Anton Paar, Austria) under the condition of 25 °C. The apparent viscosities of freshly prepared emulsions were monitored throughout from 0.1 to 100 1/s.[67]

Encapsulation efficiency was determined according to a published method.[68] The amount of essential oil in the emulsions was determined using a UV-2600 UV−vis spectrophotometer (Shimadzu, Japan) at a wavelength of 277 nm, and the release percent of essential oil from the emulsion was calculated using predetermined linear calibration curves (absorbance = 0.0147 × concentration (μg/mL) − 0.0292, R^2 = 0.9992).

Optical microscopy was used to analyze the microstructure of emulsion droplets. The morphology of emulsion droplets was observed using a DS-Fi2 microscope equipped with NIS Elements Imaging software Version 4.60 (Nikon, Japan). Approximately 20 μL of the diluted emulsion was placed on a glass slide, covered with a cover glass, and then placed on the microscope to observe the morphology under a suitable magnification.[69]

4.5. Release Measurement and Determination of Effective Diffusivity. The release mechanism of the loaded essential oil from the emulsion was evaluated based on the change in concentration as a function of time during dialysis of emulsion with excess solvent.[70] Briefly, 1 mL of each emulsion was transferred into a cellulose dialysis bag (11.5 mm × 80.0 mm), and the bag was suspended in 500 mL of a 20% (v/v) ethanol solution and then placed in a 37 °C water bath with magnetic stirring at 200 rpm. Release behavior was monitored by collecting 3 mL of dialysate at regular time intervals and replaced with an equal volume of a fresh 20% (v/v) ethanol solution. The release of essential oil was determined at 277 nm using a UV−vis spectrometer as described before. Finally, the release profiles of essential oil in emulsions were obtained by plotting the cumulative release as a function of time.

The release characteristics of essential oil with emulsion droplets could be considered the diffusion of the active ingredient from the oil core toward the interface. Therefore, Fick's second law of diffusion was used to clarify the experimental release data. In this model, the dependent parameter was the fraction of the cumulative amount of essential oil (M_t), which related the concentration gradient in real time to both initial and equilibrium concentrations.[71]

$$\frac{dM_t}{dt} = D_{eff}\frac{d^2M_t}{dx^2}$$

where D_{eff} is the effective diffusivity, t is the release time, and x is the spatial dimension.

When the internal oil core ingredient diffusion was assumed to be the main control mechanism, and the diffusion occurred

https://doi.org/10.1021/acsomega.1c06666
ACS Omega 2022, 7, 8651−8664

in one dimension within an infinite plate, the mathematical equation could be approximately simplified as follows

$$\frac{M_t}{M_0} = 1 - \frac{6}{\pi^2}\exp\left(-\frac{\pi^2 D_{\text{eff}}}{r^2}t\right)$$

Or its linear form in logarithmic transformation as follows

$$\ln\left(1 - \frac{M_t}{M_0}\right) = \ln\frac{6}{\pi^2} - \frac{\pi^2 D_{\text{eff}}}{r^2}t$$

where M_0 is the release at infinite time, equal to the amount of essential oil encapsulated in the emulsion droplets, and r is the equivalent radius of emulsion droplets measured by laser diffraction.

4.6. Mathematical Modeling of the Release Curves. Several commonly used release models, including zero-order, first-order, Higuchi, Hixson−Crowell, Peppas, and Page models, were selected to evaluate the best model representing the release of essential oil in all emulsions. These models are listed in Table 6. These models were extensively used in the drug release of emulsions, inclusion complexes, microcapsules, and other microparticle systems. Based on the release model, the release mechanism of drugs could be elucidated, which could guide the drug design and finally achieve the desired release behavior. The fit quality and accuracy of the release models were evaluated by the square of the correlation coefficient (R^2).[72]

Table 6. Mathematical Models Selected to Fit the Release Kinetics[a]

model	equation	linear transformation
zero-order	$Q_t = kt + Q_0$	
first-order	$Q'_t = Q_0 e^{-kt}$	$\ln Q_t = Q_0 - kt$
Higuchi	$Q_t = k\sqrt{t} + n$	
Hixson−Crowell	$\sqrt[3]{Q_0} - \sqrt[3]{Q'_t} = kt$	
Peppas	$Q_t = kt^n$	$\ln Q_t = \ln k + n \ln t$
Page	$Q_t = e^{-kt^n}$	$\ln \ln(Q_t) = \ln(-k) + n \ln t$

[a] k, n—model parameters; Q_t—the amount of essential oil released at time t; Q_0—the initial amount of essential oil; and $Q't$—the amount of essential oil remained in the emulsion at time t ($Q't = Q_0 - Q_t$).

4.7. Statistical Analysis. The data were presented as mean values and standard deviations. Statistical analyses of differences between the values were determined via the analysis of variance (ANOVA) procedure of the SPSS 26.0 program, and $P < 0.05$ was considered to be statistically significant.

■ ASSOCIATED CONTENT

Supporting Information

The Supporting Information is available free of charge at https://pubs.acs.org/doi/10.1021/acsomega.1c06666.

Immiscibility behavior of camellia oil and water (PDF)

■ AUTHOR INFORMATION

Corresponding Author

Liangshan Ming − *Institute for Advanced Study, Key Laboratory of Modern Preparation of TCM, Ministry of Education, Research Center for Differentiation and Development of TCM Basic Theory, Jiangxi University of Chinese Medicine, Nanchang 330004, China;* orcid.org/0000-0003-2971-822X; Phone: +86-0971-87142859; Email: jazmaster@163.com, mingls@jxutcm.edu.cn

Authors

Zhe Li − *Institute for Advanced Study, Key Laboratory of Modern Preparation of TCM, Ministry of Education, Research Center for Differentiation and Development of TCM Basic Theory, Jiangxi University of Chinese Medicine, Nanchang 330004, China*

Xiaoxia Jiang − *Institute for Advanced Study, Key Laboratory of Modern Preparation of TCM, Ministry of Education, Research Center for Differentiation and Development of TCM Basic Theory, Jiangxi University of Chinese Medicine, Nanchang 330004, China*

Hongning Liu − *Institute for Advanced Study, Key Laboratory of Modern Preparation of TCM, Ministry of Education, Research Center for Differentiation and Development of TCM Basic Theory, Jiangxi University of Chinese Medicine, Nanchang 330004, China*

Ziheng Yao − *Institute for Advanced Study, Key Laboratory of Modern Preparation of TCM, Ministry of Education, Research Center for Differentiation and Development of TCM Basic Theory, Jiangxi University of Chinese Medicine, Nanchang 330004, China*

Ao Liu − *Institute for Advanced Study, Key Laboratory of Modern Preparation of TCM, Ministry of Education, Research Center for Differentiation and Development of TCM Basic Theory, Jiangxi University of Chinese Medicine, Nanchang 330004, China*

Complete contact information is available at: https://pubs.acs.org/10.1021/acsomega.1c06666

Author Contributions

[†]Z.L. and X.J. contributed equally to this work.

Notes

The authors declare no competing financial interest.

■ ACKNOWLEDGMENTS

This research was funded by the National Natural Science Foundation of China (82003953), Jiangxi Provincial Natural Science Foundation (20202BAB216039 and 20212BAB216009), Science and Technology Research Project of Jiangxi Administration of Traditional Chinese medicine (2021A327), Science and Technology Research Project of Jiangxi Provincial Department of Education (GJJ190688 and GJJ201252), and 2020−2022 Young Talents Support Project of Chinese Society of Chinese Medicine (2020-QNRC2-07).

■ REFERENCES

(1) Zhang, J.; Zhang, J.; Wang, S.; Yi, T. Development of an oral compound Pickering emulsion composed of nanocrystals of poorly soluble ingredient and volatile oils from Traditional Chinese Medicine. *Pharmaceutics* **2018**, *10*, No. 170.

(2) Feng, X.; Sun, Y.; Yang, Y.; Zhou, X.; Cen, K.; Yu, C.; Xu, T.; Tang, X. Zein nanoparticle stabilized Pickering emulsion enriched with cinnamon oil and its effects on pound cakes. *LWT* **2020**, *122*, No. 109025.

(3) Huang, Y.; Liu, H.; Liu, S.; Li, S. Cinnamon cassia oil emulsions stabilized by chitin nanofibrils: Physicochemical properties and antibacterial activities. *J. Agric. Food Chem.* **2020**, *68*, 14620−14631.

(4) Wu, X.; Li, X.; Yang, L.; Yuan, L.; Xu, Z.; Xu, J.; Ge, L.; Mu, C.; Li, D. Stability enhanced Pickering emulsions based on gelatin and dialdehyde starch nanoparticles as simple strategy for structuring liquid oils. *Food Bioprocess Technol.* **2021**, *14*, 1600−1610.

(5) Heyse, A.; Kraume, M.; Drews, A. The impact of lipases on the rheological behavior of colloidal silica nanoparticle stabilized Pickering emulsions for biocatalytical applications. *Colloids Surf., B* **2020**, *185*, No. 110580.
(6) Briceño-Ahumada, Z.; Soltero-Martínez, J. F. A.; Castillo, R. Aqueous foams and emulsions stabilized by mixtures of silica nanoparticles and surfactants: A state-of-the-art review. *Chem. Eng. J. Adv.* **2021**, *7*, No. 100116.
(7) Griffith, C.; Daigle, H. Manipulation of Pickering emulsion rheology using hydrophilically modified silica nanoparticles in brine. *J. Colloid Interface Sci.* **2018**, *509*, 132−139.
(8) Macedo Fernandes Barros, F.; Chassenieux, C.; Nicolai, T.; de Souza Lima, M. M.; Benyahia, L. Effect of the hydrophobicity of fumed silica particles and the nature of oil on the structure and rheological behavior of Pickering emulsions. *J. Dispersion Sci. Technol.* **2019**, *40*, 1169−1178.
(9) Alison, L.; Ruhs, P. A.; Tervoort, E.; Teleki, A.; Zanini, M.; Isa, L.; Studart, A. R. Pickering and network stabilization of biocompatible emulsions using chitosan-modified silica nanoparticles. *Langmuir* **2016**, *32*, 13446−13457.
(10) Knapik-Kowalczuk, J.; Kramarczyk, D.; Chmiel, K.; Romanova, J.; Kawakami, K.; Paluch, M. Importance of Mesoporous Silica Particle Size in the Stabilization of Amorphous Pharmaceuticals-The case of simvastatin. *Pharmaceutics* **2020**, *12*, No. 384.
(11) Ming, L.; Huang, H.; Jiang, Y.; Cheng, G.; Zhang, D.; Li, Z. Quickly identifying high-risk variables of ultrasonic extraction oil from multi-dimensional risk variable patterns and a comparative evaluation of different extraction methods on the quality of Forsythia suspensa seed oil. *Molecules* **2019**, *24*, No. 3445.
(12) Ren, X.; Xu, Z.; Deng, R.; Huang, L.; Zheng, R.; Kong, Q. Peppermint essential oil suppresses geotrichum citri-aurantii growth by destructing the cell structure, internal homeostasis, and cell cycle. *J. Agric. Food Chem.* **2021**, *69*, 7786−7797.
(13) Li, Z.; Ding, Y.; Huang, H.; Wang, K.; Wu, J.; Zhu, L.; Liao, Z.; Ming, L. Study of β- cyclodextrin differential encapsulation of essential oil components by using mixture design and NIR: Encapsulation of α-pinene, myrcene, and 3-carene as an example. *J. Chin. Pharm. Sci.* **2021**, *30*, 524−537.
(14) del Carmen Razola-Díaz, M.; Guerra-Hernandez, E. J.; Garcia-Villanova, B.; Verardo, V. Recent developments in extraction and encapsulation techniques of orange essential oil. *Food Chem.* **2021**, *354*, No. 129575.
(15) Balan, G. C.; Paulo, A. F. S.; Correa, L. G.; Alvim, I. D.; Ueno, C. T.; Coelho, A. R.; Ströher, G. R.; Yamashita, F.; Sakanaka, L. S.; Shirai, M. A. Production of wheat flour/PBAT active films incorporated with oregano oil microparticles and its application in fresh pastry conservation. *Food Bioprocess Technol.* **2021**, *14*, 1587−1599.
(16) Jiang, Y.; Wang, D.; Li, F.; Li, D.; Huang, Q. Cinnamon essential oil Pickering emulsion stabilized by zein-pectin composite nanoparticles: Characterization, antimicrobial effect and advantages in storage application. *Int. J. Biol. Macromol.* **2020**, *148*, 1280−1289.
(17) Zhou, Y.; Sun, S.; Bei, W.; Zahi, M. R.; Yuan, Q.; Liang, H. Preparation and antimicrobial activity of oregano essential oil Pickering emulsion stabilized by cellulose nanocrystals. *Int. J. Biol. Macromol.* **2018**, *112*, 7−13.
(18) Sun, R.; Song, G.; Zhang, H.; Zhang, H.; Chi, Y.; Ma, Y.; Li, H.; Bai, S.; Zhang, X. Effect of basil essential oil and beeswax incorporation on the physical, structural, and antibacterial properties of chitosan emulsion based coating for eggs preservation. *LWT* **2021**, *150*, No. 112020.
(19) Shin, J.; Seo, S.-M.; Park, I.-K.; Hyun, J. Larvicidal composite alginate hydrogel combined with a Pickering emulsion of essential oil. *Carbohydr. Polym.* **2021**, *254*, No. 117381.
(20) Han, W.; Zhou, G.; Gao, D.; Zhang, Z.; Wei, Z.; Wang, H.; Yang, H. Experimental analysis of the pore structure and fractal characteristics of different metamorphic coal based on mercury intrusion-nitrogen adsorption porosimetry. *Powder Technol.* **2020**, *362*, 386−398.
(21) He, X.; Cheng, Y.; Hu, B.; Wang, Z.; Wang, C.; Yi, M.; Wang, L. Effects of coal pore structure on methane-coal sorption hysteresis: An experimental investigation based on fractal analysis and hysteresis evaluation. *Fuel* **2020**, *269*, No. 117438.
(22) Jin, H.; Fan, C.; Wei, W.; Zhang, D.; Sun, J.; Cao, C. Evolution of pore structure and produced gases of Zhundong coal particle during gasification in supercritical water. *J. Supercrit. Fluids* **2018**, *136*, 102−109.
(23) Bao, Y.; Zhang, Y.; Liu, P.; Ma, J.; Zhang, W.; Liu, C.; Simion, D. Novel fabrication of stable Pickering emulsion and latex by hollow silica nanoparticles. *J. Colloid Interface Sci.* **2019**, *553*, 83−90.
(24) Mura, P.; Valleri, M.; Fabianelli, E.; Maestrelli, F.; Cirri, M. Characterization and evaluation of different mesoporous silica kinds as carriers for the development of effective oral dosage forms of glibenclamide. *Int. J. Pharm.* **2019**, *563*, 43−52.
(25) Zeng, Q.; Wan, W.; Chen, L. Enhanced mechanical and electrochemical performances of silica-based coatings obtained by electrophoretic deposition. *ACS Appl. Mater. Interfaces* **2019**, *11*, 24308−24317.
(26) Huang, D.; Guo, C.; Zhang, M.; Shi, L. Characteristics of nanoporous silica aerogel under high temperature from 950 °C to 1200 °C. *Mater. Design* **2017**, *129*, 82−90.
(27) Ming, L.; Zhe, L.; Wu, F.; Wang, Y.; Du, R.; Zhao, L.; Feng, Y. Research on compaction behavior of pharmaceutical powders based on surface free energy. *Acta Pharm. Sin.* **2017**, *52*, 1170−1177.
(28) Ge, S.; Xiong, L.; Li, M.; Liu, J.; Yang, J.; Chang, R.; Liang, C.; Sun, Q. Characterizations of Pickering emulsions stabilized by starch nanoparticles: Influence of starch variety and particle size. *Food Chem.* **2017**, *234*, 339−347.
(29) Almitani, K. H.; Abu-Hamdeh, N. H.; Etedali, S.; Abdollahi, A.; Goldanlou, A. S.; Golmohammadzadeh, A. Effects of surfactant on thermal conductivity of aqueous silica nanofluids. *J. Mol. Liq.* **2021**, *327*, No. 114883.
(30) Macedo Fernandes Barros, F.; Chassenieux, C.; Nicolai, T.; de Souza Lima, M. M.; Benyahia, L. Effect of the hydrophobicity of fumed silica particles and the nature of oil on the structure and rheological behavior of Pickering emulsions. *J. Dispersion Sci. Technol.* **2019**, *40*, 1169−1178.
(31) Pichot, R.; Spyropoulos, F.; Norton, I. T. O/W emulsions stabilised by both low molecular weight surfactants and colloidal particles: The effect of surfactant type and concentration. *J. Colloid Interface Sci.* **2010**, *352*, 128−135.
(32) Pichot, R.; Spyropoulos, F.; Norton, I. T. Mixed-emulsifier stabilised emulsions: Investigation of the effect of monoolein and hydrophilic silica particle mixtures on the stability against coalescence. *J. Colloid Interface Sci.* **2009**, *329*, 284−291.
(33) Martinović, A.; Cavoski, I. The exploitation of cornelian cherry (Cornus mas L.) cultivars and genotypes from Montenegro as a source of natural bioactive compounds. *Food Chem.* **2020**, *318*, No. 126549.
(34) Benavent-Gil, Y.; Rosell, C. M. Comparison of porous starches obtained from different enzyme types and levels. *Carbohydr. Polym.* **2017**, *157*, 533−540.
(35) Björkegren, S.; Nordstierna, L.; Torncrona, A.; Palmqvist, A. Hydrophilic and hydrophobic modifications of colloidal silica particles for Pickering emulsions. *J. Colloid Interface Sci.* **2017**, *487*, 250−257.
(36) Li, J.-E.; Nie, S.-P.; Xie, M.-Y.; Li, C. Isolation and partial characterization of a neutral polysaccharide from Mosla chinensis Maxim. cv. Jiangxiangru and its antioxidant and immunomodulatory activities. *J. Funct. Foods* **2014**, *6*, 410−418.
(37) Cao, L.; Si, J. Y.; Liu, Y.; Sun, H.; Jin, W.; Li, Z.; Zhao, X. H.; Pan, R. L. Essential oil composition, antimicrobial and antioxidant properties of Mosla chinensis Maxim. *Food Chem.* **2009**, *115*, 801−805.
(38) Pudziuvelyte, L.; Stankevicius, M.; Maruska, A.; Petrikaite, V.; Ragazinskiene, O.; Draksiene, G.; Bernatoniene, J. Chemical composition and anticancer activity of Elsholtzia ciliata essential oils and extracts prepared by different methods. *Ind. Crop. Prod.* **2017**, *107*, 90−96.

https://doi.org/10.1021/acsomega.1c06666
ACS Omega 2022, 7, 8651−8664

(39) Li, Z.; Jiang, X.; Yao, Z.; Chen, F.; Zhu, L.; Liu, H.; Ming, L. Chitosan functionalized cellulose nanocrystals for stabilizing Pickering emulsion: Fabrication, characterization and stability evaluation. *Colloids Surf., A* **2022**, *632*, No. 127769.
(40) Chou, T.-Y.; Lu, Y.-F.; Inbaraj, B. S.; Chen, B.-H. Camelia oil and soybean-camelia oil blend enhance antioxidant activity and cardiovascular protection in hamsters. *Nutrition* **2018**, *51*−*52*, 86−94.
(41) Pharmacopoeia, *Pharmacopoeia of China*; China Medicine Science and Technology Press, 2020.
(42) Lv, S.; Zhou, H.; Bai, L.; Rojas, O. J.; McClements, D. J. Development of food-grade Pickering emulsions stabilized by a mixture of cellulose nanofibrils and nanochitin. *Food Hydrocolloids* **2021**, *113*, No. 106451.
(43) Zhao, Z.; Lu, M.; Mao, Z.; Xiao, J.; Huang, Q.; Lin, X.; Cao, Y. Modulation of interfacial phenolic antioxidant distribution in Pickering emulsions via interactions between zein nanoparticles and gallic acid. *Int. J. Biol. Macromol.* **2020**, *152*, 223−233.
(44) Souza, A. G.; Ferreira, R. R.; Paula, L. C.; Setz, L. F. G.; Rosa, D. S. The effect of essential oil chemical structures on Pickering emulsion stabilized with cellulose nanofibrils. *J. Mol. Liq.* **2020**, *320*, No. 114458.
(45) Raut, J. S.; Karuppayil, S. M. A status review on the medicinal properties of essential oils. *Ind. Crop. Prod.* **2014**, *62*, 250−264.
(46) Sufi-Maragheh, P.; Nikfarjam, N.; Deng, Y.; Taheri-Qazvini, N. Pickering emulsion stabilized by amphiphilic pH-sensitive starch nanoparticles as therapeutic containers. *Colloids Surf., B* **2019**, *181*, 244−251.
(47) Spyropoulos, F.; Clarke, C.; Kurukji, D.; Norton, I. T.; Taylor, P. Emulsifiers of Pickering-like characteristics at fluid interfaces: Impact on oil-in-water emulsion stability and interfacial transfer rate kinetics for the release of a hydrophobic model active. *Colloids Surf., A* **2020**, *607*, No. 125413.
(48) Huang, X.-N.; Zhou, F.-Z.; Yang, T.; Yin, S.-W.; Tang, C.-H.; Yang, X.-Q. Fabrication and characterization of Pickering High Internal Phase Emulsions (HIPEs) stabilized by chitosan-casein-ophosphopeptides nanocomplexes as oral delivery vehicles. *Food Hydrocolloids* **2019**, *93*, 34−45.
(49) Vemavarapu, C.; Surapaneni, M.; Hussain, M.; Badawy, S. Role of drug substance material properties in the processibility and performance of a wet granulated product. *Int. J. Pharm.* **2009**, *374*, 96−105.
(50) Li, Z.; Xian, J.; Wu, F.; Lin, X.; Shen, L.; Feng, Y. Development of TCM-based composite particles for direct compaction by particle design. *Powder Technol.* **2018**, *338*, 481−492.
(51) Fu, M.; Perlman, M.; Lu, Q.; Varga, C. Pharmaceutical solid-state kinetic stability investigation by using moisture-modified Arrhenius equation and JMP statistical software. *J. Pharm. Biomed. Anal.* **2015**, *107*, 370−377.
(52) Choi, K. H.; Lee, D.; Park, B. J. Interpretation of interfacial interactions between lenticular particles. *J. Colloid Interface Sci.* **2020**, *580*, 592−600.
(53) Xi, Y.; Luo, Z.; Lu, X.; Peng, X. Modulation of cyclodextrin particle amphiphilic properties to stabilize Pickering emulsion. *J. Agric. Food Chem.* **2018**, *66*, 228−237.
(54) Tan, S.; Zhong, C.; Langrish, T. Encapsulation of caffeine in spray-dried micro-eggs for controlled release: The effect of spray-drying (cooking) temperature. *Food Hydrocolloids* **2020**, *108*, No. 105979.
(55) Zainuddin, N.; Ahmad, I.; Zulfakar, M. H.; Kargarzadeh, H.; Ramli, S. Cetyltrimethylammonium bromide-nanocrystalline cellulose (CTAB-NCC) based microemulsions for enhancement of topical delivery of curcumin. *Carbohyd. Polym.* **2021**, *254*, No. 117401.
(56) Li, Z.; Wen, W.; Chen, X.; Zhu, L.; Cheng, G.; Liao, Z.; Huang, H.; Ming, L. Release characteristics of an essential oil component encapsulated with cyclodextrin shell matrices. *Curr. Drug Deliv.* **2021**, *18*, 487−499.
(57) Zhu, W. F.; Zhu, L.; Li, Z.; Wu, W. T.; Guan, Y. M.; Chen, L. H.; Mao, Z. X.; Ming, L. S. The novel use of PVP K30 as templating agent in production of porous lactose. *Pharmaceutics* **2021**, *13*, No. 814.
(58) Ming, L.; Li, Z.; Wu, F.; Du, R.; Feng, Y. A two-step approach for fluidized bed granulation in pharmaceutical processing: Assessing different models for design and control. *PLoS One* **2017**, *12*, No. e0180209.
(59) Li, Y.; Zhao, G.; Hong, B.; Zhao, S.; Han, X.; Pera-Titus, M. Unraveling particle size and roughness effects on the interfacial catalytic properties of Pickering emulsions. *Colloids Surf., A* **2020**, *599*, No. 124800.
(60) Salama, I. E.; Paul, A. Emulsions of fluorinated oils stabilised by fluorinated silica nanoparticles. *Colloids Surf., A* **2016**, *494*, 125−138.
(61) Neville, F.; Dixon, L.; Hyde, E. D. E. R. A comparative study of hydrophobic silica particle synthesis. *Adv. Powder Technol.* **2016**, *27*, 2317−2323.
(62) Liu, Y.; Liu, W.; Feng, D.; Wei, Z.; Guo, T.; Wang, G.; Song, Z. Structure-induced superhydrophilicity of silica membranes through hybridization and self-assembly of different dispersed nanoparticles. *J. Mol. Struct.* **2019**, *1177*, 26−32.
(63) Rosenberger, L.; von Essen, C.; Khutia, A.; Kühn, C.; Georgi, K.; Hirsch, A. K. H.; Hartmann, R. W.; Badolo, L. Crystalline sponge affinity screening: A fast tool for soaking condition optimization without the need of X-ray diffraction analysis. *Eur. J. Pharm. Sci.* **2021**, *164*, No. 105884.
(64) Hadidi, M.; Pouramin, S.; Adinepour, F.; Haghani, S.; Jafari, S. M. Chitosan nanoparticles loaded with clove essential oil: Characterization, antioxidant and antibacterial activities. *Carbohyd. Polym.* **2020**, *236*, No. 116075.
(65) Wu, F.; Deng, J.; Hu, L.; Zhang, Z.; Jiang, H.; Li, Y.; Yi, Z.; Ngai, T. Investigation of the stability in Pickering emulsions preparation with commercial cosmetic ingredients. *Colloids Surf., A* **2020**, *602*, No. 125082.
(66) Griffith, C.; Daigle, H. Destabilizing Pickering emulsions using fumed silica particles with different wettabilities. *J. Colloid Interface Sci.* **2019**, *547*, 117−126.
(67) Qi, W.; Li, T.; Zhang, Z.; Wu, T. Preparation and characterization of oleogel-in-water pickering emulsions stabilized by cellulose nanocrystals. *Food Hydrocolloids* **2021**, *110*, No. 106206.
(68) Razavi, M. S.; Golmohammadi, A.; Nematollahzadeh, A.; Fiori, F.; Rovera, C.; Farris, S. Preparation of cinnamon essential oil emulsion by bacterial cellulose nanocrystals and fish gelatin. *Food Hydrocolloids* **2020**, *109*, No. 106111.
(69) Griffith, C.; Daigle, H. On the shear stability of water-in-water Pickering emulsions stabilized with silica nanoparticles. *J. Colloid Interface Sci.* **2018**, *532*, 83−91.
(70) Asabuwa Ngwabebhoh, F.; Ilkar Erdagi, S.; Yildiz, U. Pickering emulsions stabilized nanocellulosic-based nanoparticles for coumarin and curcumin nanoencapsulations: In vitro release, anticancer and antimicrobial activities. *Carbohydr. Polym.* **2018**, *201*, 317−328.
(71) Vega-Gálvez, A.; Miranda, M.; Diaz, L. P.; Lopez, L.; Rodriguez, K.; Di Scala, K. Effective moisture diffusivity determination and mathematical modelling of the drying curves of the olive-waste cake. *Bioresour. Technol.* **2010**, *101*, 7265−7270.
(72) Zeng, J.; Ming, L.; Wang, J.; Huang, T.; Liu, B.; Feng, L.; Xue, M.; Chen, J.; Du, R. F.; Feng, Y. Empirical prediction model based process optimization for droplet size and spraying angle during pharmaceutical fluidized bed granulation. *Pharm. Dev. Technol.* **2020**, *25*, 720−728.

https://doi.org/10.1021/acsomega.1c06666
ACS Omega 2022, 7, 8651−8664